The Journal of the Korean Society of Oceanography
Vol. 31, No. 3, pp. 123-133, September 1996

Shallow Water Tides in the Seas around Korea

LAKSHMI H. KANTHA[1], INKWEON BANG[2], JEI-KOOK CHOI[1] AND MOON-SIK SUK[2]
[1]*Department of Aerospace Engineering Sciences, Colorado Center for Astrodynamics Research, University of Colorado, Boulder, CO 80309-0431*
[2]*Korea Ocean Research and Development Institute, Ansan, Korea*

We describe here the shallow water tides in the seas around Korea, obtained from a nonlinear barotropic model of tides in a domain encompassing the Yellow Sea, the East China Sea and the East Sea (Sea of Japan). As expected, the shallow water tides are large in the shallow marginal areas around the Yellow Sea, with the M4 tide reaching amplitudes as high as 10 cm near the Korean coast, and quite small in the East Sea. However, we also find that the regions east of the Yangtze River (126°E, 30°N) in the East China Sea also sustain large shallow water tides, with M_4 amplitudes reaching 5 cm. Such large shallow water tides are an important component of altimeter-measured sea levels and should not be ignored in any altimetric analyses of the Yellow Sea and the East China Sea. This study also highlights the desirability of very high resolution models to derive accurate shallow water tides in coastal regions.

INTRODUCTION

Satellite-borne altimeters are one of the most important global ocean measurement and monitoring techniques available to modern oceanographers. While the U.S. Navy's GEOdetic SATellite (GEOSAT) mission in the mid-eighties firmly established its value, the full potential of satellite altimetry was not realized until the launch of the NASA/CNES TOPEX/Poseidon precision altimeter in 1992. The dual-frequency TOPEX altimeter, with a bore-sighted microwave radiometer, has enabled the sea surface topography to be measured and monitored to an unprecedented degree of accuracy (3-5 cm rms. overall, Fu *et al.*, 1995). Since the ephemerides of the satellite can now be determined to an accuracy of a few centimeters by precision tracking/modeling, and other means such as GPS (Global Positioning System), the errors in orbit determination are no longer the major source of inaccuracy in determining the long-term sea surface height (SSH) variability in the global oceans. Instead, the residual errors due to inaccurate determination of the tidal SSH has become one of the three major remaining sources of error in modern altimetry, the other two being departures from inverse barometric response to atmospheric pressure fluctuations and the electromagnetic (EM) bias.

Errors due to inaccurate subtraction of tides are particularly serious in shallow water. While modern tidal models (and precision altimetry itself) can now provide tides in most of the global oceans quite accurately for altimetric analyses (Desai and Wahr, 1995), it is still difficult to compute tides accurately in many shallow coastal and marginal seas around the world (Le Provost *et al.*, 1994; Kantha, 1995). The principal problem is the inaccurate databases (Kantha, 1995) and small spatial scales that require high resolution tidal models, and the importance of shallow water tides in many shallow water regions around the world. Shallow water tides are generated in shallow water by nonlinear interaction of primary tides, principally the semidiurnal M_2 and S_2 components. There are 6 shallow water tides of possible interest to altimetry, M_4, MS_4, M_6, $2MS_6$, $2SM_2$ and S_4 (Table 1). Of these M_4 and MS_4 are probably the most important. While in principle, it is possible to extract any shallow water

Table 1. Characteristics of the six shallow water tedes (taken from Pugh, 1987)

Constituent	Generated by	Angular Speed	degree/hour
M_4	M_2	$M_2 + M_2$	57.9682
MS_4	M_2, S_2	$M_2 + S_2$	58.9841
M_6	M_2	$M_2 + M_2 + M_2$	86.9523
$2MS_6$	M_2, S_2	$M_2 + M_2 + S_2$	87.9682
$2SM_2$	M_2, S_2	$S_2 + S_2 - M_2$	31.0159
S_4	S_2	$S_2 + S_2$	60.0000

tide from altimetric measurements themselves using along-track tidal extraction techniques, in practice, the high degree of spatial variability of shallow water tides near the coast, improper sampling and small amplitudes make this technique useful perhaps only for M_4. A high resolution nonlinear numerical barotropic model is a better alternative. This article addresses the problem of computing shallow water tides numerically in shallow coastal shelves and seas around the world, with the seas around Korea as an example.

Korea is surrounded on three sides by seas, the Yellow Sea in the west, the East Sea in the East, and the East China Sea to the south. The most obvious difference between the Yellow Sea and the East Sea (Sea of Japan) is the water depth. The Yellow Sea is a bowl-shaped shallow basin with a maximum depth of less than 100 m while the East Sea is a deep mini-basin with a maximum depth of 3500 m and hardly any continental shelf. This topographic difference leads to marked differences in their response to atmospheric and astronomical forcing. Tides are one of the largest in the world in the Yellow Sea, exceeding a range of 6 m near the Korean coast, but are quite small, although non-negligible for altimetric purposes, in the East Sea. This means that the shallow water tides also reach high amplitudes in the Yellow Sea, especially in the shallow coastal regions near Korea and China.

TIDAL MODEL

A vertically-integrated, fully nonlinear barotropic data-assimilative tidal model, the global version of which is described by Kantha (1995) is used in this study to compute shallow water tides numerically. The model incorporates direct astronomical forcing and the regional version derives the conditions needed on open boundaries from global tidal models such as Desai and Wahr (1995) and Kantha (1995). The reader is referred to Kantha (1995) for a detailed description and Kantha *et al.* (1995) for some altimetric and geophysical applications (see also http://www.cast.msstate.edu/Tides2D). The model can simulate any combination of primary, long-term and shallow water tides and for this study, we have run the model for M_2 and S_2.

The tides are quite complex in the Korea/Tsushima Strait connecting the East Sea and the East China Sea. It is therefore preferable to model the entire Korea Seas region to avoid having to prescribe the needed boundary conditions in the region of the Strait. This is the strategy we have employed. While direct astronomical forcing is relatively unimportant in the Yellow Sea, it is retained in the model for accuracy and because of inclusion of the East Sea in the model domain, where directly forced tides are not much smaller than the co-oscillating tides. Figure 1 shows the model domain and the inclined model grid (rotated 35° counterclockwise). The model domain extends from Taiwan Strait near the South China Sea to Tatar Strait near the Sea of Okhotsk. The resolution is ~20 km. Bathymetry has been derived from a combination of 5' DBDB5 global bathymetric data base and charts from local sources.

The model was driven by tides derived from Desai and Wahr (1995) global model prescribed on the open boundaries. Taiwan Strait was assumed closed. While Kantha (1995) relied primarily on assimilation of altimetric and coastal tide gage data for accurate simulation of tides, we describe here runs both with and without data assimilation. The modeling strategy is to first simulate M_2 and S_2 individually to obtain the best possible results without assimilation and then in combination to derive shallow water tides. The former (for M_2 and S_2) were run for 20 days and the last 10 days were used for estimating the coamplitude/cophase of the tidal sea level fluctuations. Residual currents were also derived, averaged over 10 tidal cycles. The shallow water tide simulations (for M_4, MS_4, M_6,

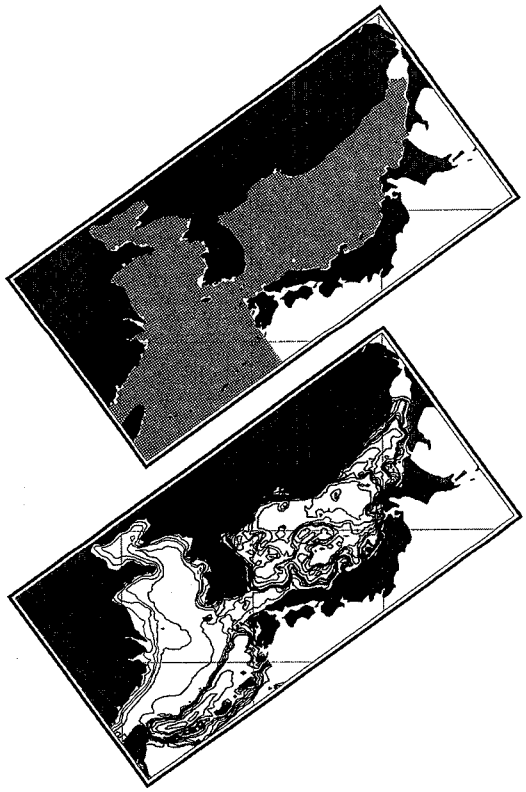

Fig. 1. Model grid system (upper) and topography (lower, thick lines in the Yellow Sea and East China Sea are 50 m and 100 m).

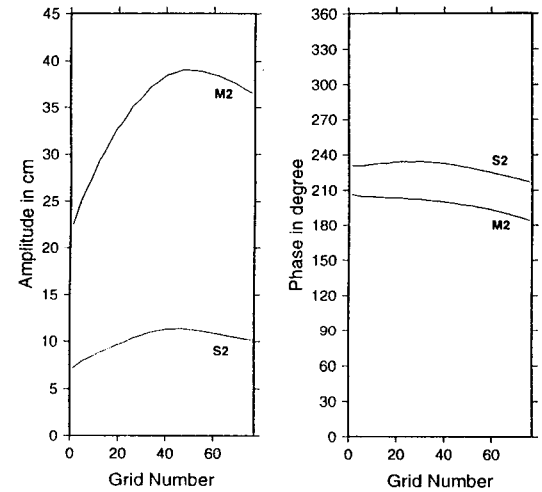

Fig. 2. Prescribed amplitudes and phases of M_2 and S_2 along the open boundary. Grid number increases from southwest to northeast. Phases here and also in other figures are referred to 135° E.

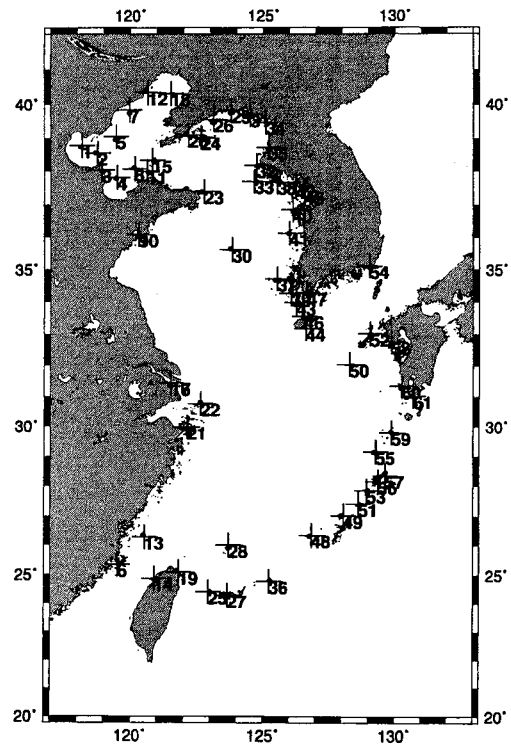

Fig. 3. Tide gage station locations.

$2MS_6$, $2SM_2$, and S_4) were done for a total of 40 days and the last 29 days of hourly data saved at all model grid points were used to derive the coamplitude/cophase of both primary and compound constituents by harmonic analysis. Model was ramped up over 5 days.

Figure 2 shows the M_2 and S_2 amplitudes and phases prescribed at the open boundary. The amplitudes had to be adjusted downwards by 25% and 50% respectively, from Desai and Wahr (1995) values to obtain reasonable agreement with tide gage data in the model run without any data assimilation. Figure 3 shows the location of the 61 coastal tide gages, located within 0.1° from the model grid, selected for assessment of model results. There are 7 coastal tide gage stations where all 6 shallow water tides are available for comparison with model results Unfortunately, we know of no data away from the coast that can be used to assess model results in open water.

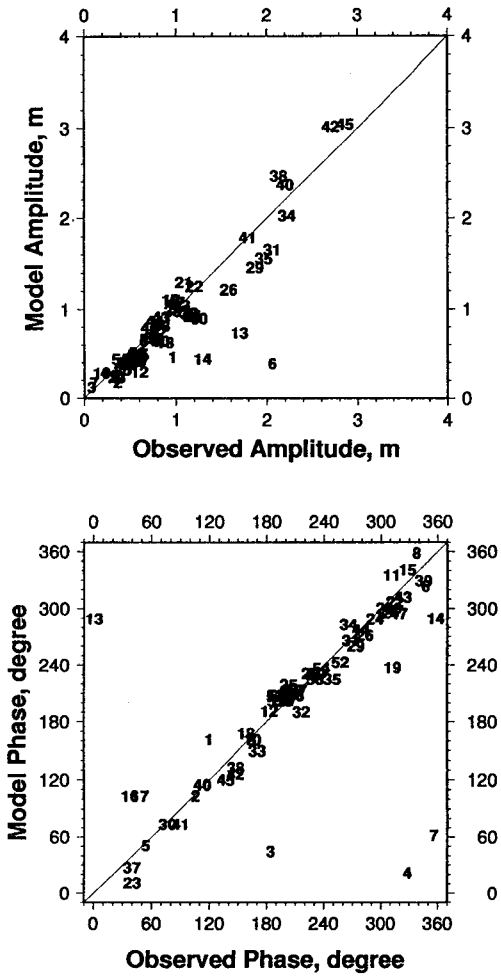

Fig. 4. Scatterplots of modeled and observed amplitudes and phases of M_2 at tide gage stations.

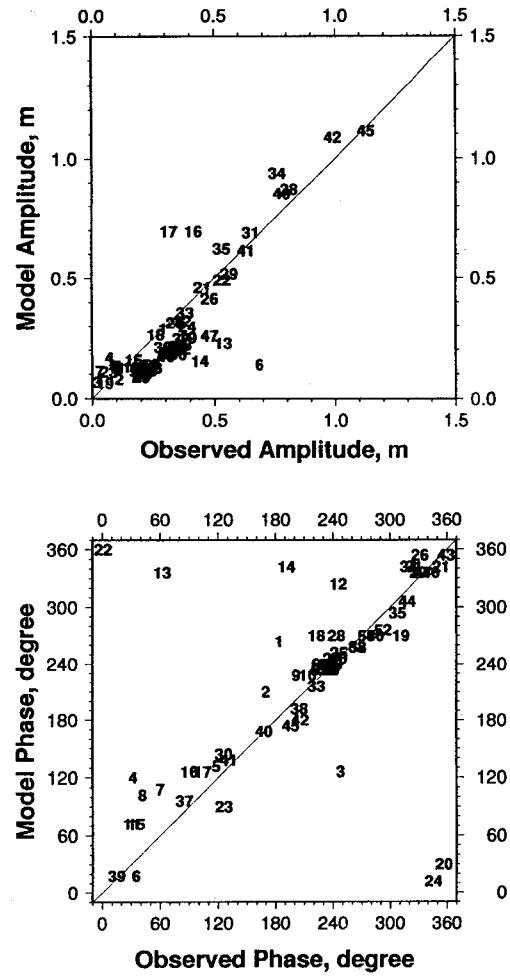

Fig. 5. Scatterplots of modeled and observed amplitudes and phases of S_2 at tide gage stations.

MPDEL RESULTS

Figures 4 and 5 show scatterplots comparing observed tidal coamplitudes and cophases for M_2 and S_2 at the various coastal tide gage stations with those modeled without assimilation. The overall agreement is quite good, considering the ~20 km resolution of the model. For a quantitative comparison, the distance between the observed and modeled points in the complex plane as defined by Foreman *et al.* (1993) is used:

$$D = [(A_o \cos\phi_o - A_m \cos\phi_m)^2 + (A_o \sin\phi_o - A_m \sin\phi_m)^2]^{1/2}$$

where A_o and A_m are observed and modeled amplitudes, ϕ_o and ϕ_m are the corresponding phases. The value of D is shown for M_2 and S_2 and is plotted in Figure 6. Also shown is the ratio of D to the observed amplitude. Large differences are found at Stations 6, 13 and 14, located in and near the closed Taiwan Strait. Also the computed amplitudes for both M_2 and S_2 are smaller than observed (Figure 4) because of the closed boundary. At some stations in the Gulf of Pohai and the Gulf of Liautung (stations 3, 4, and 7), the ratio is high and this is because their amplitudes are small and phase changes are large over short distance due to the proximity of the nearby amphidromic point. At stations 16 and 17

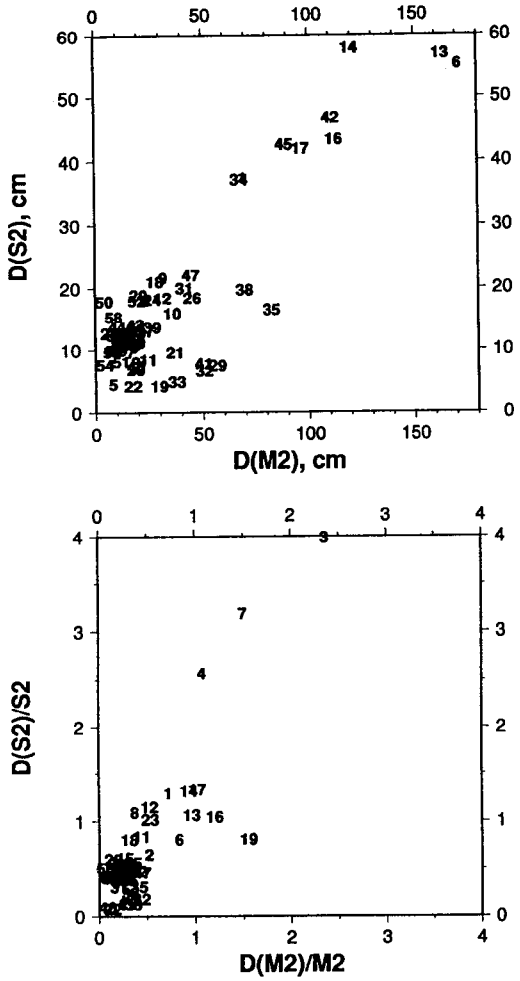

Fig. 6. Distances between modeled and observed points in the complex plane (upper) and their ratio to the observed amplitudes (lower).

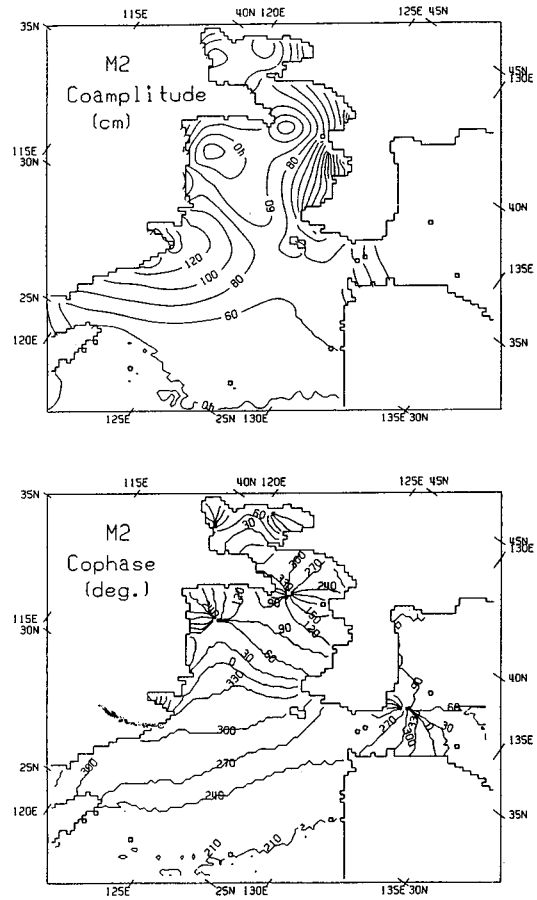

Fig. 7. Coamplitude and cophase distribution for M_2.

(Shanghai) both the distances and the ratios are large; however the quality of the observational data is uncertain. At almost all other points the distances are less than ~50 cm for M_2 and ~10 cm for S_2 and the ratio to the observed amplitudes are less than 0.5 for both M_2 and S_2.

We will now compare the horizontal patterns of M_2 coamplitudes and cophases to the numerical modeling results presented by Choi (1990) and Kang *et al.* (1991) and the observations of Fang (1994). Choi's results are only for the Yellow Sea and East China Sea, but the resolution is very high (1/15 degree), while Kang *et al.* (1991) included the East Sea and the resolution is 1/6 degree. The coamplitudes and cophase patterns are similar to these two previous modeling efforts, and the amphidromic points are well-defined in the Yellow Sea (Figure 7).

However in the East Sea, only the amphidrome near Korea is reproduced whereas there exists another amphidrome near Tatar Strait. Our model domain includes only the southern part of the Tatar Strait, and the Soya and Tsugaru Straits are closed. The amphidrome north of Korea Strait in the East Sea is located a bit farther north than in Fang (1994), but is in agreement with the amphidrome of Kang *et al.* (1991). Cophase distribution of S_2 is similar to M_2 and the position of the amphidromes are almost the same as those of M_2 (Figure 8). The magnitudes are only about one third of M_2 but the distribution is similar to M_2.

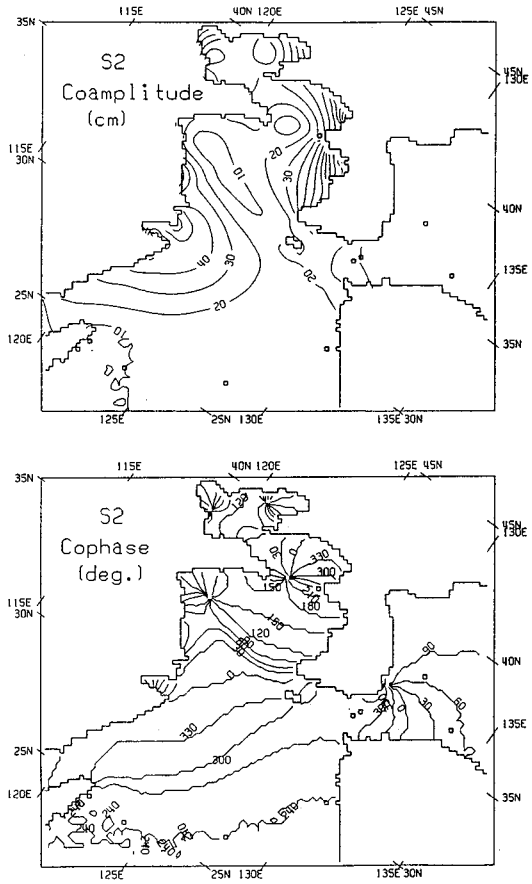

Fig. 8. Coamplitude and cophase distribution for S_2.

Figures 9 and 10 are streak plots of the residual currents by M_2 and S_2, respectively. Each arrow in these figures represents artificial drifter track released at a grid point and traced for 100 days. New positions of drifters are computed at one day interval. Dominant feature of M_2 residual current is the outflow from the Yellow Sea through the deep portion between Chinese coast and Cheju Island. This outflow is mainly supplied from the southward flow in the central Yellow Sea and it is connected to the southwestward flow in the East China Sea although the strength becomes very weak in this region. South of 34° N along the Chinese coast there is strong offshore flow and it changes direction to southeastward to join the outflow. In the S_2 residual current this offshore flow from the Chinese coast is the main source of outflow from the Yellow Sea. S_2 residual

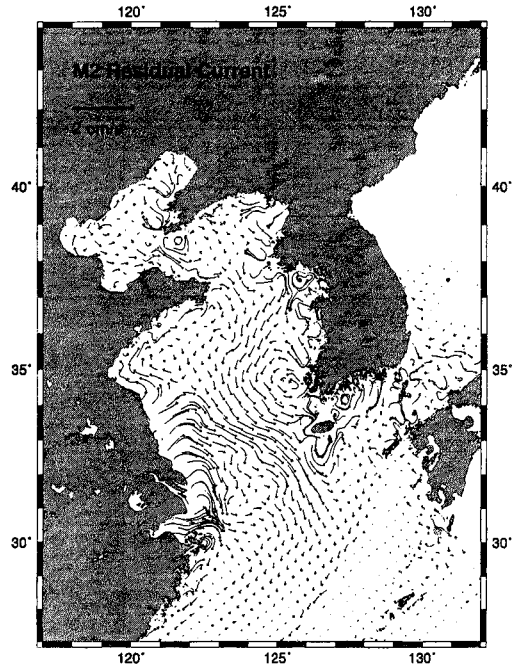

Fig. 9. Streak plots of M_2 residual current.

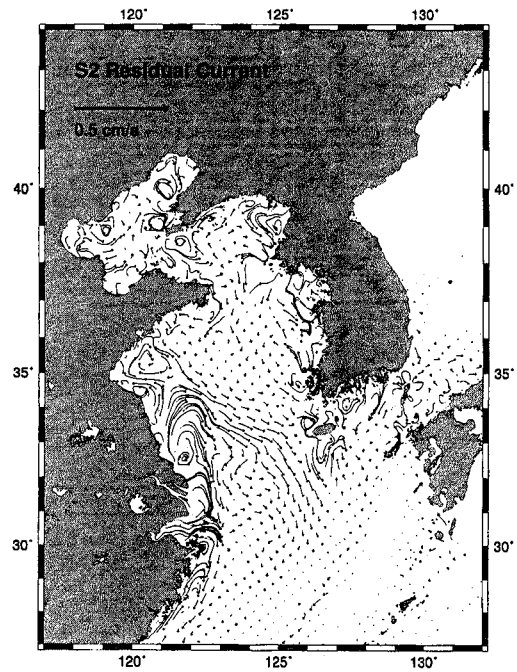

Fig. 10. Streak plots of S_2 residual current.

current pattern is similar to M_2 but the magnitude is much smaller than that of M_2 (about 1/5 of M_2).

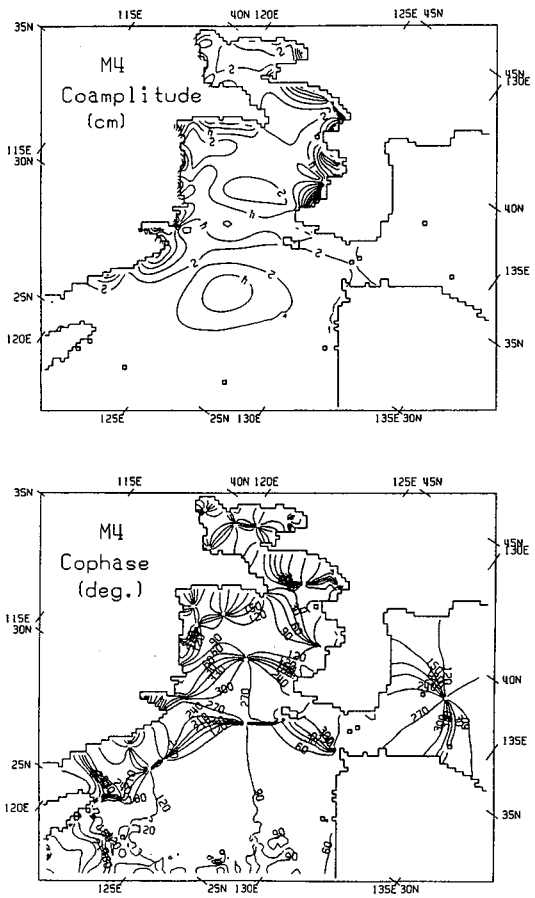

Fig. 11. Coamplitude and cophase distribution for M_4.

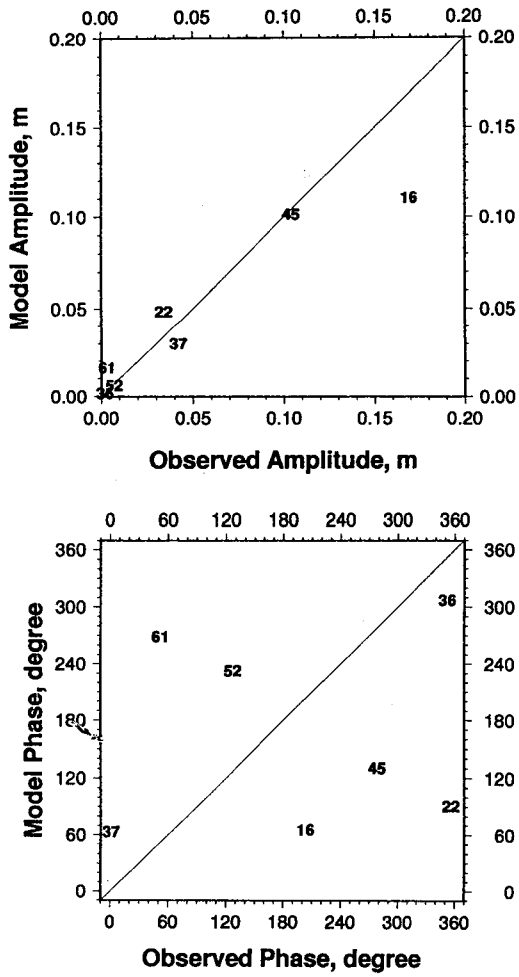

Fig. 12. Scatterplots of modeled and observed amplitudes and phases of M_4 at tide gage stations.

We present next the coamplitudes and cophases of six shallow water constituents arising from the interaction of M_2 and S_2. M_4 is the largest of them and we can compare our result with Choi's (1990) numerical computations. In his model, the M_4 amplitude is high, more than 5 cm, in the region where M_2 amplitude is high, i.e., along the west coast of Korea and the Chinese coast south of 34° N. Our results also show high values in the same region (Figure 11). One interesting feature that was not noted in Choi (1990) is the high value region east of the Yangtze River (126°E, 30°N). Amplitudes are higher than 4 cm in this region and it is isolated from other high value regions which are located near the coast. Such a disconnection would indicate that it is generated locally and in that case topography would be a major candidate for that (Pugh, 1987). Water depths in this region are between 50 m and 100 m and horizontal gradient of water depth is highest in this depth range in the East China Sea (Figure 1). Therefore, the rapid change in water depth could be a generating factor for this isolated high value region. However, it is not clear why an ioslated high exist only in this region while regions with water depths between 50 m and 100 m extend from Taiwan to the west of Cheju Island. In most of Yellow and East China Seas, the amplitudes are higher than 2 cm and values higher than 10 cm are found along the west coast of Korea. M_4 is not generated from the tidal wave propagation from the Pacific as in the case of M_2, but from the nonlinear interaction

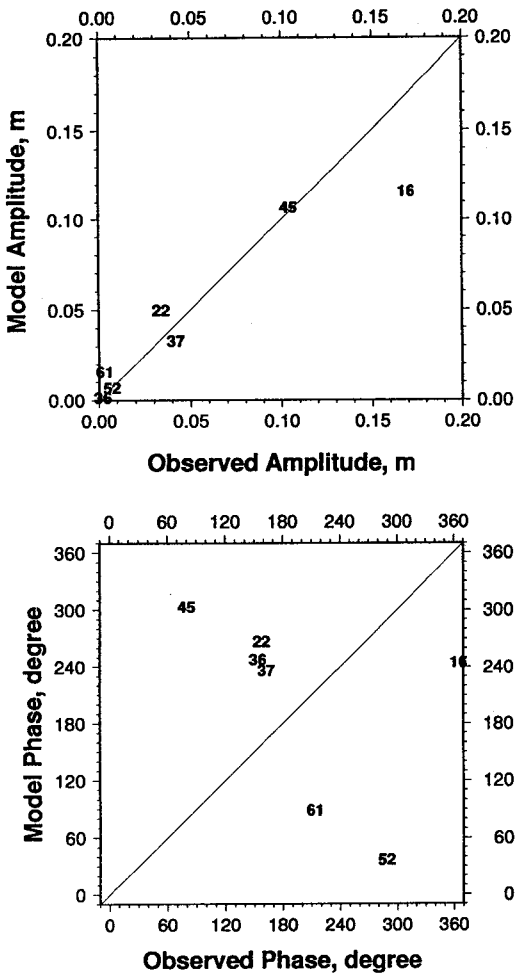

Fig. 13. Same as Figure 12, but with data assimilation.

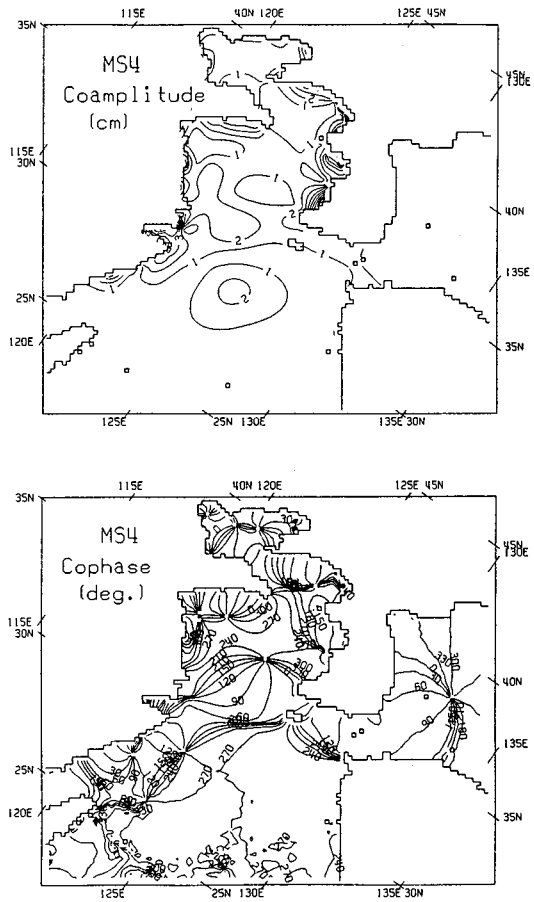

Fig. 14. Coamplitude and cophase distribution for MS_4.

of M_2 with itself. This is made clear by the lack of cophase lines that are parallel to the open boundary which are present in M_2 distributions. High amplitude regions of M_2 must also be those of M_4. From the phase distributions, we can say that in the Kyunggi Bay the M_4 tide generated near the coast propagates in the offshore direction and that generated near Kunsan propagates southward along the coast. Number of amphidromes are more than double those of M_2 because M_4 has half the period of M_2 and consequently shorter wavelengths. Some amphidromes have cophase lines rotating clockwise while all M_2 amphidromes have counterclockwise rotation.

Comparison of the computed values with the observed values shows good agreement of the amplitudes but not the phases (Figure 12). Even the assimilation of the limited coastal gage data into the model does not improve the agreement (Figure 13). It is likely that a higher model resolution and assimilation of data on shallow water tides at least at some points away from the coast might be necessary for improved results. It is possible to derive at least some shallow water tides from observations by accurate altimeters such as TOPEX. Disagreement of the computed phases with the observed phases was also noted in the northwest European continental shelf (Davis, 1996) and he attributed it to the rapid change of phase from one grid point to the next due to its shorter wavelength

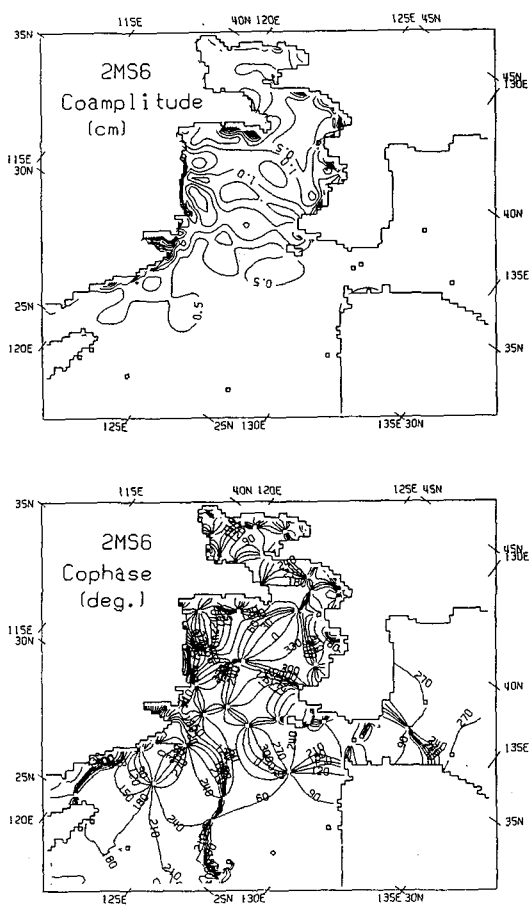

Fig. 15. Coamplitude and cophase distribution for $2MS_6$.

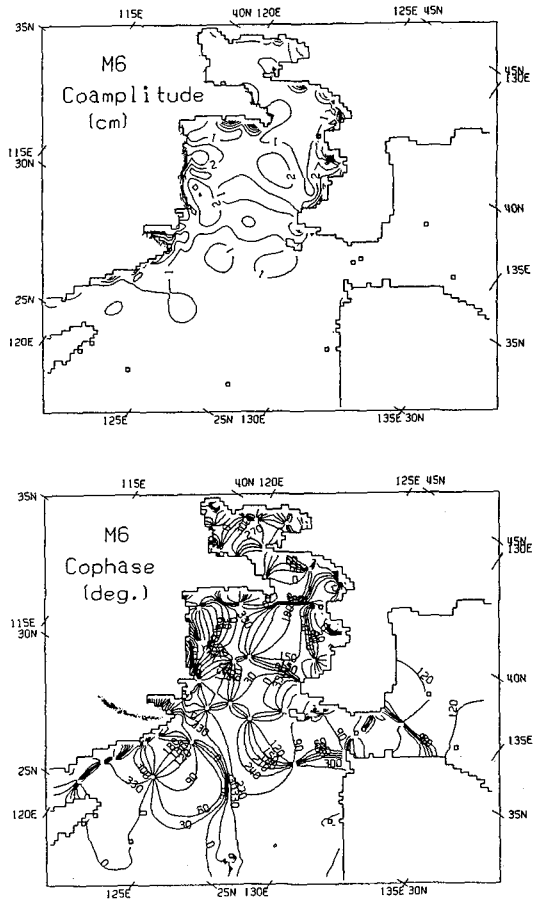

Fig. 16. Coamplitude and cophase distribution for M_6.

than M_2.

MS_4 has the angular speed of sum of M_2 and S_2 and is a quarter-diurnal constituent. MS_4 is the most important of compound tides arising from M_2 and S_2 (Dronkers, 1964). MS_4 coamplitude pattern is similar to the pattern of M_4 but the magnitude is about half of M_4 (Figure 14). Since M_2 is larger than S_2 it appears that M_2 affects the MS_4 distribution more than S_2. The next important compound tide is the six-diurnal constituent $2MS_6$. Its amplitude is smaller than 2 cm except along the west coast of Korea (Figure 15). M_6 is an overtide of M_2 and its amplitude is a bit larger than $2MS_6$ but smaller than the most important compound tide MS_4 (Figure 16). Component $2SM_2$ has amplitudes less than 1 cm everywhere except in some coastal regions of Korea (Figure 17). The smallest of the six constituents is S_4 and its amplitude is about half that of $2SM_2$ (Figure 18).

CONCLUSIONS

For the first time, shallow water tidal constituents arising from the nonlinear interaction of M_2 and S_2 have been computed and presented in the Yellow Sea, the East China Sea and the East Sea. Our model adopted a rotated grid to include all the seas around Korea. Although the model is barotropic and the resolution is not as high as in other works (Choi, 1990; KORDI, 1995), the agreement of the modeled M_2 and S_2 with observed data is fairly good.

The most important shallow water constituent M_4 also shows a good agreement of modeled amplitudes

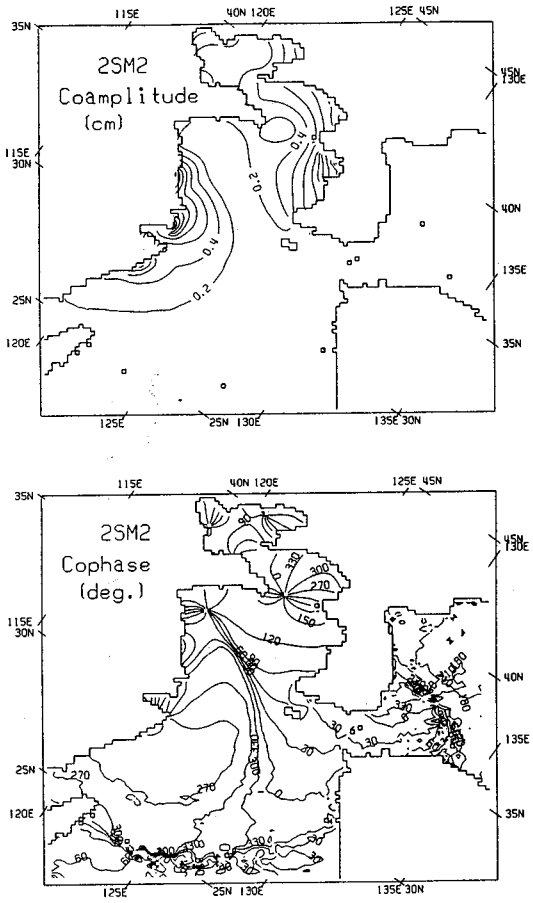

Fig. 17. Coamplitude and cophase distribution for $2SM_2$.

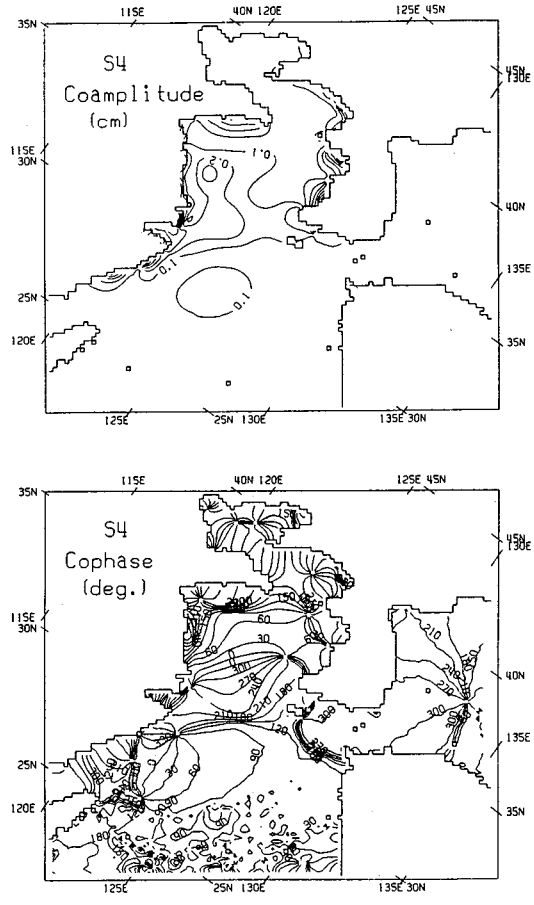

Fig. 18. Coamplitude and cophase distribution for S_4.

with observed ones. M_4 amplitudes are larger than 2 cm in most of the Yellow Sea and East China Sea so that it cannot be excluded from the detiding process in the analysis of altimetry data in these regions. The modeled M_4 phase shows large differences with observed ones. The causes are two-fold: 1. The relatively poor grid resolution; a higher resolution is desirable for the quarter-diurnal and higher constituents because of their shorter wavelengths. Resolution is particularly critical near the coast because a large phase distortion can occur due to local geographic features, which are not resolved by a coarse resolution model. 2. Lack of shallow water tide data off the coast for assimilation. Altimetry itself holds the promise of deriving at least the major shallow water tides and at least at the crossover points, accurately, in regions like the Yellow Sea.

The other constituents (MS_4, $2MS_6$, M_6) also have amplitudes larger than 1 cm in wide areas of the Yellow Sea so that their exclusion can cause significant errors if sea-level change of a couple of centimeters is dynamically important. In fact, the dynamically important subtidal signals in the Yellow Sea are not expected to exceed several centimeters since the sea level anomalies do not exceed 10 cm in the East Sea (Bang *et al.*, 1996). This makes it particularly important to derive accurate shallow water tides in the Yellow Sea.

REFERENCES

Bang, I., L.H. Kantha, J.-K. Choi, C. Horton, M. Clifford,

M.-S. Suk, K.-I. Chang, S.Y. Nam, H.-J. Lie, 1996. A hindcast experiment in the East Sea (Sea of Japan). *La mer*, **34**: 35-57.

Choi, B.H., 1984. A three-dimensional model of the East China Sea. In: Ocean Hydrodynamics of the Japan and East China Seas, edited by T. Ichiye, Elsevier, 209-224.

Choi, B.H., 1990. Development of fine-grid numerical tidal models of the Yellow Sea and the East China Sea, *J. Coastal Ocean Engineers*, **2**: 231-244.

Davis, A.M., 1986. A three-dimensional model of the northwest European continental shelf with application to the M_4 tide. *J. Phys. Oceanogr.*, **16**: 797-813.

Desai, S.D. and J.M Wahr, 1995. Empirical ocean tide models estimated from TOPEX/POSEIDON satellite altimetry. *J. Geophys. Res.*, **100**: 25,104-25,122.

Dronkers, J.J., 1964. Tidal Computations in Rivers and Coastal Waters. North Holland Publ. Co., Amsterdam, 518 pp.

Fang, G., 1994. Tides and tidal currents in East China Sea, Huanghai Sea and Bohai Sea. In: Oceanography of China Seas, Vol. 1, edited by D. Zhou, Y.-B. Liang, and C.-K. Zeng (C.K. Tseng), Kluwer Academic Publishers, 101-112.

Foreman, M.G.G., R.F. Henry, R.A. Walters, and V.A. Ballantyne, 1993. A finite element model for tides and resonance along the north coast of British Columbia, *J. Geophys. Res.*, **98**: 2,509-2,532.

Kang, S.K., Lee S.-R., and Yum K.-D., 1991. Tidal computations of the East China Sea, the Yellow Sea and the East Sea. In: Oceanography of Asian Marginal Seas, edited by K. Takano, Elsevier, 25-48.

Kantha, L.H., 1995. Barotropic tides in the global oceans from a nonlinear tidal model assimilating altimetric tides 1. Model description and result. *J. Geophys. Res.*, **100**: 25,283-25,308.

Kantha, L.H., C. Tierney, J.W. Lopez, S.D. Desai, M.E. Parke and L. Drexler, 1995. Barotropic tides in the global oceans from a nonlinear tidal model assimilating altimetric tides 2. Altimetric and geophysical implications. *J. Geophys. Res.*, **100**: 25,309-25,317.

KORDI, 1995. Ocean circulation and material flux of East China Sea (first year)-Eastern East China Sea. KORDI report BSPN 00257-812-1, 371-394.

Pugh, D.T., 1987. Tides, Surges and Mean Sea-Level. John Wiley & Sons, Chichester, 472 pp.